

Elliptical solitons in the dissipative Lugiato-Lefever equationA. V. Yulin *Department of Physics, ITMO University, Saint Petersburg 197101, Russia*A. V. Andrianov  and E. A. Anashkina *Institute of Applied Physics of the Russian Academy of Sciences, Nizhny Novgorod 603950, Russia*

(Received 19 July 2022; accepted 12 October 2022; published 9 November 2022)

The formation and stability of dissipative solitons in the vector Lugiato-Lefever model are considered for the case when only one of the field components (polarization) is excited by the external coherent pump. It is shown that linearly polarized solitons can be destabilized because of the growth of the excitations belonging to the orthogonal polarization. Vector (elliptically polarized) solitons bifurcating from linearly polarized ones are found, and the stability and dynamics of the vector solitons are studied.

DOI: [10.1103/PhysRevA.106.053507](https://doi.org/10.1103/PhysRevA.106.053507)**I. INTRODUCTION**

The Lugiato-Lefever equation provides a quite general framework for studying rich and complex dynamics in dissipative nonlinear optical systems [1]. One prominent example of such systems is dielectric optical microresonators [2]. To date, most of the theoretical works have concentrated on the scalar Lugiato-Lefever equation. A large number of diverse regimes can be observed even in steady state [3]. The scalar equation supports linearly polarized dissipative Kerr solitons, which represent a very important and sufficiently well-studied class of solutions [4]. Scalar Kerr solitons have been demonstrated in many experiments. In the frequency domain they are optical frequency combs with excellent coherent and low-noise properties desirable for manifold applications [4]. From the point of view of frequency comb generation the aforementioned dissipative solitons propagating in driven-dissipative microring waveguides can be seen as a promising alternative to other generation methods including conservative solitons in optical fibers [5–7], broadband radiation generated in vertical external-cavity surface-emitting lasers [8,9], and time delayed systems [10,11].

Moreover, spatial multiplexed (noninteracting) solitons driven by a continuous wave (CW) laser can be generated in different spatial (or polarization) mode families of a microresonator [12]. Under certain conditions, solitons generated in different mode families can interact through the Kerr nonlinearity. To analyze this problem theoretically, a vector model can be constructed based on two coupled Lugiato-Lefever equations. More generally, in systems described by two coupled Lugiato-Lefever equations nonlinear dynamics becomes very complicated and nontrivial. Very interesting and sometimes unexpected vector structures can be observed in them [13–19].

Interest in vector solitons and other vector dissipative structures in the Lugiato-Lefever model has arisen in recent years. Note that earlier vector solitons were investigated in

the framework of the nonlinear Schrödinger equation [20–23]. In addition to the significance for basic science, vector structures described by the Lugiato-Lefever equation have great prospects for the development of advanced light control technologies. An important motivating and stimulating factor for investigating such optical problems is the tremendous progress in the development of technologies and experimental methods that make it possible to implement proper systems, perform reliable measurements, and check theoretical predictions in experiments. Different types of microresonators, millimeter-sized resonators, or macroscopic fiber loop resonators can be used to observe and study the rich nonlinear dynamics of vector dissipative solitons or other vector structures with different polarization states described by two coupled Lugiato-Lefever equations. Important parameters of microresonators including eigenfrequencies, mode profiles, and dispersion can be tailored in a wide range [24] using currently developed fabrication techniques such as polishing, cutting, and laser processing, and so on [25–28].

Recently, Averlant *et al.* theoretically found the coexistence of two stable temporally separated vector solitons with different peak powers and Stokes parameters in a slightly birefringent fiber loop resonator described by *incoherently* coupled Lugiato-Lefever equations and constructed a bifurcation diagram demonstrating the large complexity of the system [13]. Suzuki *et al.* theoretically studied *incoherently* trapped microresonator solitons belonging to orthogonal mode families and excited by dual orthogonally polarized pumping [14]. The area of parameters of realistic silica rod microresonators corresponding to existence of trapped solitons was also discussed [14]. Nielsen *et al.* experimentally demonstrated the coexistence and interactions between nonlinear states including solitonic ones with different polarizations in a macroscopic fiber loop resonator [15]. Xu *et al.* experimentally demonstrated and theoretically explained the formation of spontaneously symmetry-broken temporally separated coexisting dissipative vector solitons having

asymmetric polarization states [16]. The deterministic switching between these states was also reported [16]. Spontaneous symmetry breaking and complex polarization dynamics of dissipative cavity solitons were recently reported [29]. Note that in these works [13–16], both solitonic components were driven by a CW pump.

Here we theoretically (numerically) study peculiarities of nonlinear dynamics of vector dissipative solitons pumped only in one polarization in the framework of the *coherently* coupled Lugiato-Lefever equations. First of all, we have found that under certain conditions a scalar (linearly polarized) soliton can spontaneously break into a two-component vector soliton with an elliptical polarization, which differs from the previously reported regimes using pumping into both polarizations. We have also found that there is a region of a bistability where the system can support at least two different stable vector solitons with different peak power and polarization states. Further, we have demonstrated oscillating (breather) behavior of elliptically polarized solitons having a well-known scalar analog [30,31]. Finally, we have examined the case of moving vector solitons (when the group velocity detuning of solitonic components is not equal to zero in contrast to the previously analyzed cases). The corresponding bifurcation diagrams have been discussed.

To describe nonlinear dynamics of intracavity radiation in a single spatial mode family of a microresonator, one can use a widespread mean-field model in the framework of the Lugiato-Lefever equation [4,32–36]. This model allows one to study optical frequency comb generation including dissipative soliton formation [4,32–36]. In microresonators, temporal waveforms have duration which is comparable with round-trip time. So, one should solve a periodic problem [36]. Here, to describe the dynamics of the light in the CW pumped microring with allowance for two orthogonally polarized mode families, we adopt the Lugiato-Lefever model and extend it to a vector case. Then in the basis of linear polarizations the equation reads

$$\begin{aligned} \partial_t A_{x,y} = & V_{x,y} \partial_z A_{x,y} + i D_{x,y} \partial_z^2 A_{x,y} \\ & + i[(\alpha + \beta)|A_{x,y}|^2 + \alpha|A_{y,x}|^2] A_{x,y} + i\beta A_{y,x}^* A_{x,y} \\ & + (i\delta_{x,y} - \gamma_{x,y}) A_{x,y} + f_{x,y} \end{aligned} \quad (1)$$

where t is time, z is the spatial coordinate, $A_{x,y}$ are the coherently coupled amplitudes of x and y polarizations, $\gamma_{x,y}$ are the losses in the polarizations, $\delta_{x,y}$ are the detunings of the resonant frequencies of x and y polarizations from the frequency of the pump, $v_{x,y}$ are the group velocities of the modes, $D_{x,y}$ are the dispersion of the modes, and $f_{x,y}$ are the pump amplitude for the x and y polarizations. To pose the problem we need to specify the boundary conditions that are periodic for the microring waveguides $A_{x,y}(z) = A_{x,y}(z + L)$ where L is the length of the ring. We set nonlinearity coefficients $\alpha = 2/3$ and $\beta = 1/3$, which is a natural choice if the nonlinearity dispersion can be neglected (see details in [37]). Note that in Eq. (1) not only incoherent (as, for example, in [29]) but also coherent interaction between the polarizations is taken into account.

Let us make a remark that Eq. (1) is often written in different coordinates using a slow time or a propagation distance instead of t and the fast retarded time instead of the spatial

coordinate (see for instance [29]). Within the framework of the slow varying amplitude approach all these equations are completely equivalent.

In this paper we focus on the case when the pump goes to only one of the polarizations, $f_y = 0$. Let us remark that choosing the appropriate moving reference system we can always provide that $V_x = 0$. Rescaling the time and the spatial coordinate allows us to set $\gamma_x = 1$ and $D_x = 1$. Then Eq. (1) can be written as

$$\begin{aligned} \partial_t A_x = & i\partial_z^2 A_x + (i\delta_x - 1)A_x \\ & + i\left(|A_x|^2 + \frac{2}{3}|A_y|^2\right)A_x + \frac{i}{3}A_y^2 A_x^* + f, \end{aligned} \quad (2a)$$

$$\begin{aligned} \partial_t A_y = & V\partial_z A_y + iD\partial_z^2 A_y + (i\delta_y - \gamma)A_y \\ & + i\left(|A_y|^2 + \frac{2}{3}|A_x|^2\right)A_y + \frac{i}{3}A_x^2 A_y^*. \end{aligned} \quad (2b)$$

Here for the sake of brevity we omitted the unnecessary indices denoting $V = V_y$, $D = D_y$, $\gamma = \gamma_y$, and $f = f_x$.

Let us remark that in the annular system the spatial spectrum is equidistant due to periodic boundary conditions. The “cold eigenmodes” (i.e., eigenmodes of an unloaded resonator) are the plane waves characterized by their wave vector $k_n = 2\pi/L$ where L is the resonator length and n is an integer. The frequency of the n th eigenmode is $\omega_n = v_{ph}k_n$ where v_{ph} is the phase velocity of the mode. First, the phase velocity depends on the frequency and thus the temporal spectrum of the eigenmodes is not equidistant. If in a certain range of frequencies the variation of the phase velocity is small then the temporal spectrum can be called equidistant. Secondly, the phase velocities of x and y polarizations are, in general, different. This means that the resonant frequencies of the polarizations do not coincide. However, the temporal spectra of optical solitons in microrings are equidistant [36]. This makes it possible to use optical solitons in microrings for frequency comb generation.

II. STABILITY OF LINEARLY POLARIZED SOLITONS

Equations (2) admit one component (x -polarized) solutions $A_x \neq 0$ and $A_y = 0$. In this case the dynamics of A_x is described by the scalar Lugiato-Lefever model. It is well known that for negative δ_x there may exist a bistability of spatially uniform solutions. Dissipative scalar Kerr solitons can nestle on these backgrounds, and the bifurcation diagram of the solitons emerges from the bifurcation diagram of the spatially uniform state. The bifurcation diagram can be calculated by finding the time-independent soliton solutions of (2). In this paper we did this by solving the corresponding ordinary differential equation by the well-known Newton iteration method. Let us also mention here that to study the dynamics of the fields we perform numerical simulations of (2). The simulations are done by the split-step method proven to be reliable and efficient for this kind of equations.

The solitons can be destabilized by growing perturbations belonging to the soliton polarization. Let us briefly describe the analysis of the dynamical stability of the soliton solutions. For the purpose of the paper it is convenient to do this for the vector case. To study the linear stability we look for the

solution in the form $A_{x,y} = A_{s,x,y} + a_{x,y}$ where $A_{s,x,y}$ are the x and y components of the time independent soliton solution and $a_{x,y}$ are the small corrections for both of the components. Then the linearized equations for $a_{x,y}$ take the form

$$\begin{aligned} \partial_t a_x &= i\partial_z^2 a_x + (i\delta_x - 1)a_x \\ &+ 2i\left(|A_{s,x}|^2 + \frac{1}{3}|A_{s,y}|^2\right)a_x + i\left(A_{s,x}^2 + \frac{1}{3}A_{s,y}^2\right)a_x^* \\ &+ \frac{2i}{3}(A_{s,x}A_{s,y}^* + A_{s,y}A_{s,x}^*)a_y + \frac{2i}{3}A_{s,y}A_{s,x}a_y^*, \end{aligned} \quad (3a)$$

$$\begin{aligned} \partial_t a_y &= V\partial_z a_y + iD\partial_z^2 a_y + (i\delta_y - \gamma)a_y \\ &+ 2i\left(|A_{s,y}|^2 + \frac{1}{3}|A_{s,x}|^2\right)a_y + i\left(A_{s,y}^2 + \frac{1}{3}A_{s,x}^2\right)a_y^* \\ &+ \frac{2i}{3}(A_{s,x}A_{s,y}^* + A_{s,y}A_{s,x}^*)a_x + \frac{2i}{3}A_{s,y}A_{s,x}a_x^*. \end{aligned} \quad (3b)$$

The dynamics of the small corrections is governed by the eigenvalues of the corresponding spectral problem which can be solved numerically.

Equations (3) get uncoupled in the case of linearly polarized solitons with only one (A_x) nonzero component:

$$\partial_t a_x = i\partial_z^2 a_x + (i\delta_x - 1)a_x + 2i|A_{s,x}|^2 a_x + iA_{s,x}^2 a_x^*, \quad (4a)$$

$$\begin{aligned} \partial_t a_y &= V\partial_z a_y + iD\partial_z^2 a_y + (i\delta_y - \gamma)a_y \\ &+ \frac{2i}{3}|A_{s,x}|^2 a_y + \frac{i}{3}A_{s,x}^2 a_y^*. \end{aligned} \quad (4b)$$

So the eigenmodes of the linear excursions are linearly polarized.

It is obvious that in the scalar case the small perturbations are governed by Eq. (4 a) and thus we refer the instability of a linearly polarized soliton against the perturbations of the same polarization as a scalar instability. It is known that for the detunings δ large enough the solitons in the scalar model can become unstable via Andronov-Hopf bifurcation, which gives birth to oscillating localized states. The information on the scalar soliton stability is summarized in Figs. 1(a) and 1(b) showing the bifurcation diagrams for $\delta = -3$ (without Andronov-Hopf bifurcation) and $\delta = -5$ (with Andronov-Hopf bifurcation). Calculating the bifurcation diagrams we detect the offset of the Andronov-Hopf instabilities by finding the pump value when a pair of complex conjugated eigenvalues crosses the imaginary axis.

It is important that in the vector model a linearly polarized soliton can be unstable against the perturbations belonging to another polarization. We refer to this instability described by Eq. (4 b) as a polarization instability. The polarization instability depends on the detuning δ_y , the velocity V , and the dispersion D . The area of the polarization instability in parameter plane f - δ_y is shown in Figs. 1(c) and 1(d) for $D = 1$ and $v = 0$.

The development of the polarization instability can result either in the destruction of the soliton or in the formation of a vector soliton. For some parameters small random perturbations of the initial state affect the development of the instability so that different vector solitons form. These vector soliton formation processes are illustrated in Fig. 2.

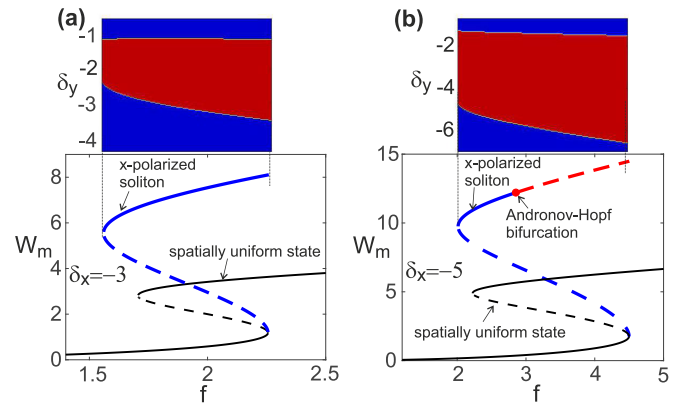


FIG. 1. The bifurcation diagrams $W_m = \max[|A_x(z)|^2]$ (peak soliton intensity as a function of pump) for linearly polarized ($A_x \neq 0$, $A_y = 0$) stationary solitons are shown in the lower parts of panels (a) and (b) for $\delta_x = -3$ and -5 correspondingly. The parts of the bifurcation curve where the solitons undergo scalar instability are shown by dashed lines. By the red dashed line we mark the region of scalar instability of Andronov-Hopf kind. The bifurcation curve of spatially uniform states is shown as a thin black curve. In the upper part of the figure there are two panels showing the regions of polarization instability of the solitons in the parameter plane f - δ_y . The regions of polarization instability of the solitons belonging to the upper part of the bifurcation diagram are shown by red color; the regions where the solitons are stable are shown by blue color.

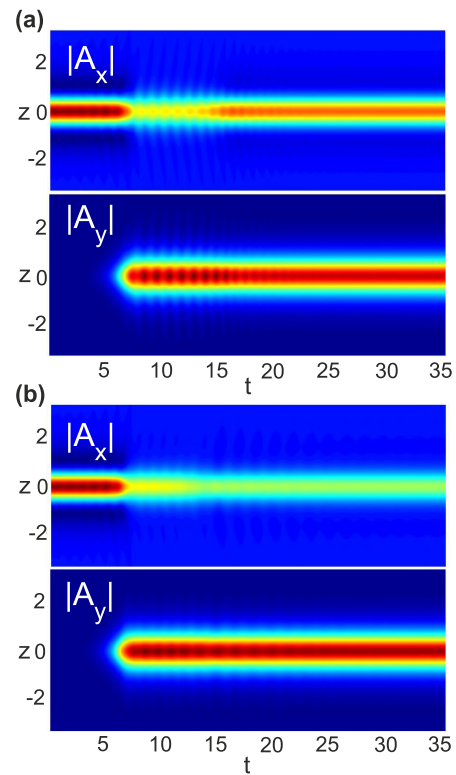


FIG. 2. The development of the instability of x -polarized solitons perturbed by weak noise. Two different scenarios of the instability development are shown in panels (a) and (b). The parameters are $\delta_x = -5$, $\delta_y = -5$, $D = 1$, and $V = 0$. The initial soliton belongs to the upper branch of the bifurcation curve and is fed by the pump $f \approx 3.482$.

As one can see the system can support stable vector solitons and, moreover, there is a region of bistability where there may exist at least two different stable vector solitons. Let us mention that the direct numerical simulations of (2) are done using the split-step method which is proven to be a fast and reliable algorithm for numerical solutions of the equations of such a kind.

III. RESTING VECTOR SOLITONS

We study systematically the bifurcations of the vector solitons starting with the case $V = 0$. The vector soliton solutions are found numerically solving the corresponding ordinary differential equations by Newton iterations and then the stability analysis is done by finding the eigenmodes of the small perturbations governed by (3).

It is found that the vector solitons with two nonzero components bifurcate from the point where polarization instability of the x -polarized soliton sets in. The bifurcation diagrams are shown in Fig. 3 for different values of δ_y and fixed $D = 1$. The stationary solutions are found by iterative procedure allowing us to find the field distribution and the velocity of the soliton. As expected, numerically found solutions confirm that for $V = 0$ the velocity of the vector soliton v_s is equal to zero with the precision of the numerical simulations. At the point where the vector solitons detach from the linearly polarized ones their second component tends, obviously, to zero. However, far from this point the energy in the second component $E_y = \int |A_y|^2 dz$ can exceed the energy of the first (directly pumped) component $E_x = \int |A_x|^2 dz$.

The vector solitons exist in the range of detunings δ_y where the x -polarized solitons are unstable (see Fig. 1). If δ_y is in the vicinity of the lower boundary of the soliton existence domain then the solitons exist in a narrow interval of the pumps close to the right edge of the bifurcation curve of the linearly polarized solitons (see Fig. 3). When δ_y approaches the lower boundary of the domain, the interval of the pumps f supporting the vector solitons shrinks to zero.

Now let us discuss what happens when δ_y goes to the upper boundary of the soliton existence domain. Then at some threshold value of δ_y another merging point of the bifurcation curves of the vector and the scalar solitons appears [see Fig. 3(d), where this second merging point is clearly seen in the inset; let us remark that all soliton branches shown in the inset are unstable, and the linearly polarized soliton becomes stable on the right of the bifurcation points against the polarization instability only].

From the numerical simulations we can conclude that the bifurcation curves of the linearly and elliptically polarized solitons get closer to each other and the intensity of the second polarization component of the elliptically polarized soliton decreases when δ_y goes to the upper boundary of the existence domain. With further decrease of δ_y , the merging points go towards each other and finally the bifurcation diagram of the vector solitons collapses.

As one can see in Figs. 2 and 3, the vector solitons can be bistable so that there are two stable vector solitons supported by the same pump. In particular, Fig. 2 shows the evolution of the unstable linearly polarized soliton marked by a magenta

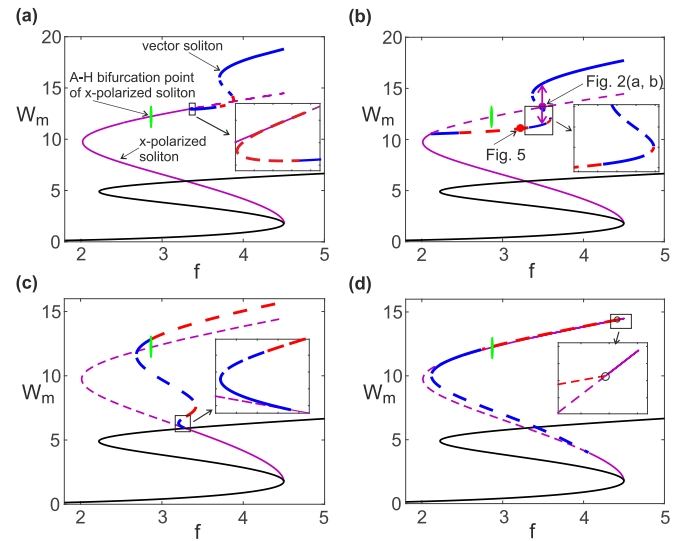


FIG. 3. Bifurcation diagrams of vector solitons for $\delta_y = -6$ (a), $\delta_y = -5$ (b), $\delta_y = -3$ (c), and $\delta_y = -1.52$ (d) by the thicker blue and red lines. The parameter W_m is the maximum of the total intensity defined as $W_m = \max[|A_x|^2 + |A_y|^2]$. The stable parts of the bifurcation curves are shown by the solid blue line, the dashed blue lines correspond to the solitons with dominating instability having pure real eigenvalue, and the dashed red lines are the case when the dominating instability is of Andronov-Hopf kind. The thinner magenta lines show the bifurcation curves of the x -polarized solitons. The solid part of the magenta lines means that the solitons do not exhibit *polarization instability* (but can be unstable against the perturbations having the same polarization as the soliton); the dashed magenta lines correspond to the polarization unstable solitons. The vertical green ellipse marks the point where scalar Andronov-Hopf bifurcation of linearly polarized solitons sets in (the solitons are unstable right of this point). The thinner black lines show the bifurcation diagrams of the spatially uniform states. The magenta arrows in panel (b) symbolically show the transformation of an unstable x -polarized soliton to one of two possible stable vector solitons. These arrows indicate the points on the bifurcation curve corresponding to the vector solitons. The other parameters are $\delta_x = -5$, $D = 1$, and $V = 0$.

circle in Fig. 3(b). The pump is then within the range of the bistability of the vector solitons and thus the final state belongs either to the upper or to the lower branches of the vector soliton bifurcation curve.

The structures of the fields in these solitons are shown in Figs. 4(a) and 4(b). One can see that the intensity of the y -polarized component can be higher than the intensity of the x -polarized component. It is also instructive to look at the polarization of the vector solitons. The normalized Stokes parameters ($St_1 = |A_x|^2 - |A_y|^2$, $St_2 = A_x^* A_y + A_x A_y^*$, and $St_3 = iA_x^* A_y - iA_x A_y^*$) are shown in Figs. 4(c) and 4(d) for the solitons belonging to the upper and to the lower parts of the dispersion curve correspondingly. One can see that in the center of the soliton the first Stokes parameter is close to zero and the third one is close to 1, which means that the field in the soliton is nearly circularly polarized (actually, of course, elliptically polarized). We would like to notice here that the equations are invariant with respect to $A_y \rightarrow -A_y$ transfor-

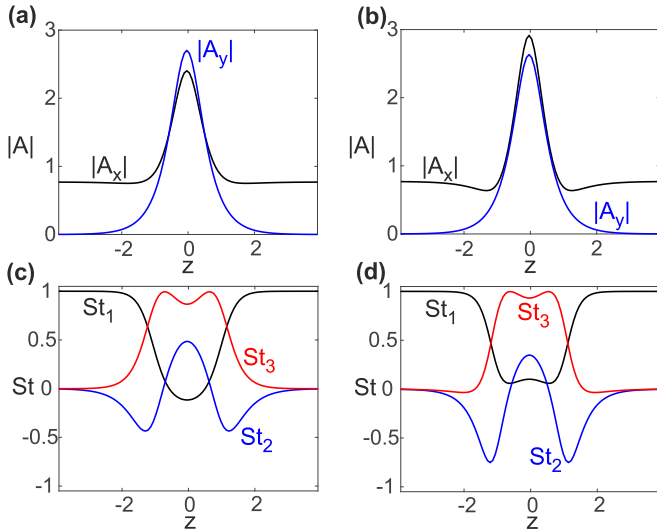


FIG. 4. The spatial distributions of the absolute values of the fields $|A_{x,y}|$ are shown in panels (a) and (b) for the vector solitons appearing due to the development of the polarization instabilities shown in Fig. 2. The corresponding Stokes parameters are shown in panels (c) and (d). Panels (a), (c) and (b), (d) are for the solitons belonging to the lower and the upper branches.

mation and thus bifurcation curves of the vector solitons are doubly degenerate.

We have examined the development of an oscillatory instability of vector solitons. It is shown that Andronov-Hopf bifurcation gives rise to oscillating (breather) vector solitons. The formation of the oscillating vector soliton looks very much like the formation of its well-known scalar counterpart [30,31] [see Fig. 5(a), showing a typical development of the oscillatory instability of vector solitons].

Because of the instability the intensities in both components of the soliton start oscillating and after some transitional phase the system reaches an oscillatory steady state [see Fig. 5(b)]. It is interesting to note that the polarization of the soliton is also oscillating [see Fig. 5(c), showing the temporal evolution of the Stokes parameters in the center of the soliton]. However, the oscillation of the polarization is not very pronounced.

IV. MOVING VECTOR SOLITONS

It is also worth discussing the case when the group velocity detuning V is not equal to zero. First, this affects the stability of the linearly polarized soliton. Secondly, vector solitons forming in this case have a nonzero velocity. In other words, the velocity of the vector solitons differs from the velocity of x -polarized solitons that move at a velocity equal to the group velocity of the x -polarized linear waves at the frequency of the pump. It should be also mentioned that in this case the vector solitons are not mirror symmetric anymore; moreover, the maxima of x - and y -polarized components do not coincide (see Fig. 6).

The typical bifurcation diagrams of vector solitons are shown in Fig. 6(a). Let us remark here that in this case the field distribution and the velocity of the soliton have to be

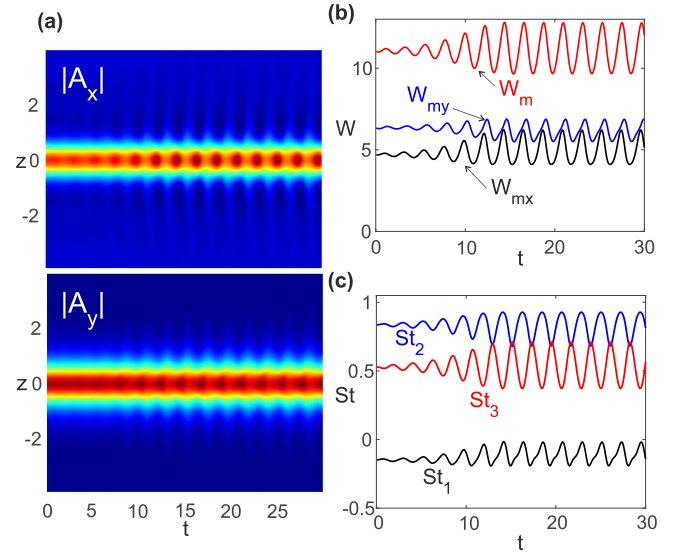


FIG. 5. The development of the Andronov-Hopf instability of the vector soliton is shown in panel (a). The initial state corresponding to the point in the bifurcation diagram Fig. 3(b) is marked by the red circle. The oscillations of the intensities maxima of the x (black line) and y (blue line) components, $W_{mx} = \max[|A_x|^2]$ and $W_{my} = \max[|A_y|^2]$ correspondingly, as well as the total intensity maximum $W_m = \max[|A_x|^2 + |A_y|^2]$ (red line) are shown in panel (b). The oscillations of Stokes parameters are illustrated in panel (c).

found self-consistently by solving the corresponding ordinary differential equations and requiring that the solution is localized. One can see that, as well as for $V = 0$, for $V \neq 0$ the vector solitons bifurcate from x -polarized ones. Figure 6(b) shows that the vector soliton moves at some velocity which depends on the intensity of the soliton. Figures 6(c), 6(d), and 6(e) show the distribution of the intensities of the soliton component, the spatial spectra of the soliton components, and the Stokes parameters. It is clearly seen that the symmetry of the soliton is broken.

It should be noted here that the displacement of the maxima of the spatial spectra in the chosen reference frame means the shift of a central temporal frequency in the laboratory reference frame. This means that the central frequencies of the x and y components of the soliton are different. However, the positions of the spectral lines in the frequency combs are the same for both polarizations.

The moving vector solitons can form from the unstable x -polarized (and resting) solitons (see Fig. 7). Figure 7(a) illustrates the case when the forming vector soliton is stable. It is seen that initially the soliton has only one nonzero component and is resting. The development of the instability transforms the soliton into a vector one and sets it in motion.

The parameters can be chosen to prevent the formation of a stable nonoscillating soliton. This case is illustrated in Fig. 7(b), showing the development of the instability of the x -polarized soliton. It is seen that at first the instability produces the second component in the soliton and the soliton begins moving at some velocity. Along with this, the oscillations of the intensities of the soliton components appear and become deeper with further development of the instability. The

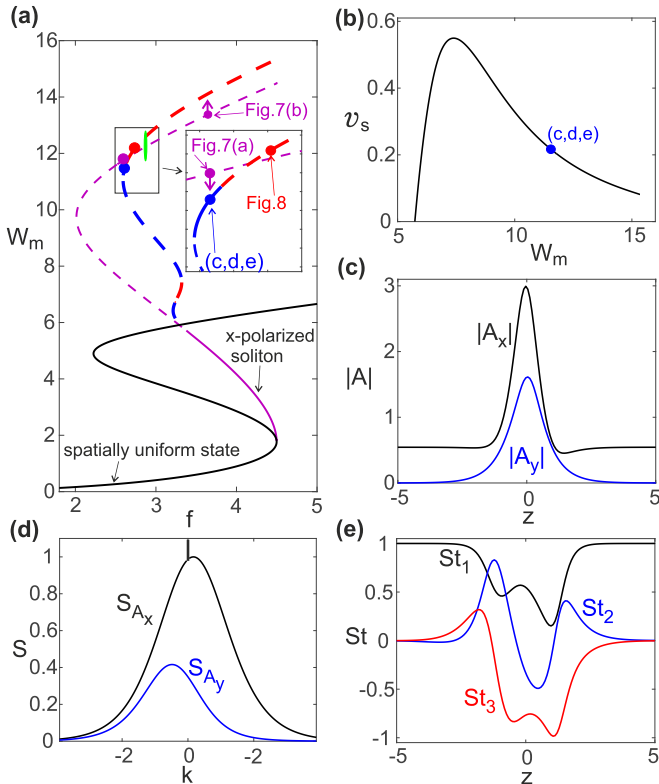


FIG. 6. The bifurcation diagram of vector solitons for $V = 1$ is shown in panel (a); $W_m = \max[|A_x|^2 + |A_y|^2]$ is the maximal total intensity of the state. The velocity of the vector soliton as a function of its maximal intensity is shown in panel (b). The energy density distributions in the soliton are shown in panel (c). Panel (d) shows the normalized spatial spectra of x and y components of the soliton. Panel (e) shows the Stokes parameters. The very narrow vertical line belonging to the spatial spectrum for the x component, which corresponds to the background in x polarization in panel (c), is artificially changed for a short thick line in panel (d). The panels (b)–(d) are for the soliton corresponding to the blue circle marked as “(c, d, e)” in panels (a) and (b). The other parameters are $\delta_x = -5$, $\delta_y = -3$, and $D = 1$.

oscillation decreases the velocity of the soliton motion and, finally, a stationary state in the form of a moving oscillating soliton forms in the system.

To show the effect of the intensity oscillations on the soliton velocity and to study Andronov-Hopf bifurcation of the vector solitons for $V \neq 0$ we performed numerical simulations of the dynamics of unstable vector solitons. So we took initial conditions in the form of a vector soliton experiencing an oscillatory instability. The typical evolution of the system is presented in Fig. 8. Figure 8(a) shows the evolution of the field in the reference frame moving with the velocity of the initial unstable soliton. So at first the velocity of the soliton in this reference frame is zero. But when the intensity oscillations become pronounced the velocity of the soliton changes. In Fig. 8(b) the instantaneous velocity of the soliton in the initial reference frame is shown by the blue line. The velocity of the soliton v_s is defined as a temporal derivative of the first moment (expectation) of the soliton intensity distribution. The black lines show the soliton velocity v_{av} averaged over its

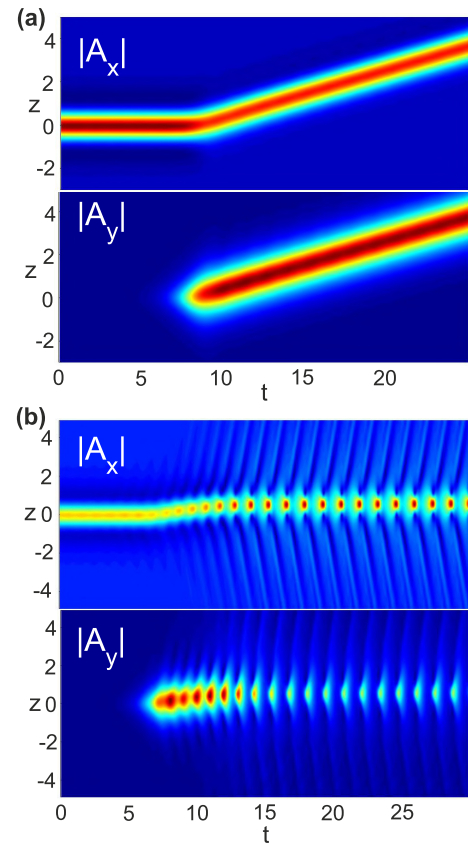


FIG. 7. The instability of x -polarized solitons and the formation of vector solitons for nonzero group velocity detuning at the frequency of the pump. Panels (a) and (b) are for the initial conditions in the form of x -polarized solitons corresponding to magenta circles marked as “Fig. 7(a)” and “Fig. 7(b)” in Fig. 6(a) correspondingly. The parameters are $\delta_x = -5$, $\delta_y = -3$, $D = 1$, and $V = 1$.

three periods of oscillations. One can see that, indeed, the velocity of the soliton decreases when the oscillations of the intensity become developed.

It is also interesting to note that at long times the average velocity v_{av} shows very slow dynamics that looks periodic. This means that the oscillating moving soliton forming from the unstable moving soliton is actually quasistable and the slow growing instability results in the appearance of spikes of the averaged soliton velocity v_{av} [see Fig. 8(c)]. We note that these spikes can be of the same origin as dissipative soliton oscillations reported in [38]. However, the detailed investigation of the dynamics of the oscillating vector solitons is out of the scope of the present paper and will be done elsewhere.

V. CONCLUSION

In this paper we consider a coherently pumped nonlinear microring with two modes of different polarizations. The consideration is restricted to the scheme where the coherent pump interacts with one of the polarization only. The simplest solutions in this case are the ones with only one nonzero component; these solutions can be found from the scalar Lugiato-Lefever model. It is well known that for the appropriate sign of the pump frequency detuning there are solutions

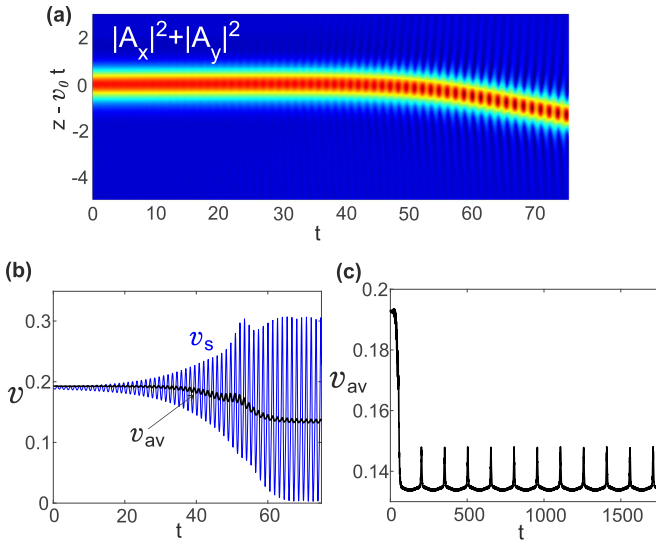


FIG. 8. The development of Andronov-Hopf instability of a vector soliton is shown in panel (a). The vertical coordinate corresponds to a reference frame moving at the velocity of the initial soliton $v_0 \approx 0.19$. The initial unstable soliton corresponds to the red circle marked as “Fig. 8” in Fig. 6(a). The dependency of an instantaneous soliton velocity v_s is shown in panel (b) by the blue line. The black line in this panel shows the soliton velocity averaged over three periods of the oscillations of the soliton intensity. The behavior of the averaged velocity over long times is presented in panel (c). The parameters are $\delta_x = -5$, $\delta_y = -3$, $D = 1$, and $V = 1$.

in the form of dissipative solitons and breathers (oscillating solitons) nestling on a background.

In this paper we examined the stability of the linearly polarized solitons in the presence of the orthogonal polarized mode. It is shown that under certain conditions small perturbations of the second polarization get amplified. The physical mechanism of the instability can be explained as follows. The linear waves of the second polarization experience both the attracting effective potential and the parametric gain created by the

soliton of the first polarization. The spatially localized states belonging to the discrete spectrum of the effective potential can be amplified by the effective gain provided that their eigenfrequencies are sufficiently close to the resonance. The growth of the localized perturbations transforms the linearly polarized soliton into an elliptically polarized one.

In this paper we systematically study the bifurcation of the elliptically polarized solitons from their linearly polarized counterparts. It is shown by linear stability analysis and by direct numerical simulations that elliptically polarized solitons can be dynamically stable. It was also demonstrated that elliptically polarized solitons can form as the result of the instability of the linearly polarized solitons. It is found that the velocity of the elliptically polarized soliton depends on the group velocities of both polarizations. So the velocities of the linearly and elliptically polarized solitons coincide only if the polarization group velocities are the same.

Oscillating elliptically polarized solitons are also found. It is demonstrated that elliptically polarized breathers can form as a result of the development of Andronov-Hopf instability of elliptically polarized solitons or directly from the decay of unstable linearly polarized solitons. It is worth mentioning that the oscillation of the elliptically polarized solitons can affect their velocity strongly.

We believe that the findings reported in this paper can contribute to a better understanding of the dynamics of the solitons in driven-dissipative systems. We also believe that the results of this paper can be used for the explanation and the optimizations of experiments on frequency comb generation in high- Q microring resonators.

ACKNOWLEDGMENTS

A.V.Y. acknowledges financial support from the Priority 2030 Academic Leadership Program and Goszadanie Grant No. 2019-1246. A.V.A. and E.A.A. acknowledge financial support from Russian Science Foundation Grant No. 20-72-10188.

-
- [1] L. A. Lugiato, F. Prati, M. L. Gorodetsky, and T. J. Kippenberg, From the Lugiato-Lefever equation to microresonator-based soliton Kerr frequency combs, *Philos. Trans. R. Soc. A* **376**, 20180113 (2018).
- [2] G. Lin, A. Coillet, and Y. K. Chembo, Nonlinear photonics with high- Q whispering-gallery-mode resonators, *Adv. Opt. Photon.* **9**, 828 (2017).
- [3] C. Godey, I. V. Balakireva, A. Coillet, and Y. K. Chembo, Stability analysis of the spatiotemporal Lugiato-Lefever model for Kerr optical frequency combs in the anomalous and normal dispersion regimes, *Phys. Rev. A* **89**, 063814 (2014).
- [4] T. J. Kippenberg, A. L. Gaeta, M. Lipson, and M. L. Gorodetsky, Dissipative Kerr solitons in optical microresonators, *Science* **361**, eaan8083 (2018).
- [5] J. M. Dudley, G. Genty, and S. Coen, Supercontinuum generation in photonic crystal fiber, *Rev. Mod. Phys.* **78**, 1135 (2006).
- [6] D. V. Skryabin and A. V. Gorbach, Looking at a soliton through the prism of optical supercontinuum, *Rev. Mod. Phys.* **82**, 1287 (2010).
- [7] J. M. Dudley and J. R. Taylor, *Supercontinuum Generation in Optical Fibers* (Cambridge University, New York, 2010).
- [8] A. C. Tropper, H. D. Foreman, A. Garnache, K. G. Wilcox, and S. H. Hoogland, Vertical-external-cavity semiconductor lasers, *J. Phys. D: Appl. Phys.* **37**, R75 (2004).
- [9] A. Laurain, M. Myara, G. Beaudoin, I. Sagnes, and A. Garnache, High power single-frequency continuously-tunable compact extended-cavity semiconductor laser, *Opt. Express* **18**, 14627 (2010).
- [10] C. Schelte, A. Pimenov, A. G. Vladimirov, J. Javaloyes, and S. V. Gurevich, Tunable Kerr frequency combs and temporal localized states in time-delayed Gires-Tournois interferometers, *Opt. Lett.* **44**, 4925 (2019).
- [11] Thomas G. Seidel, Julien Javaloyes, and Svetlana V. Gurevich, A normal form for frequency combs and localized states

- in Kerr-Gires-Tournois interferometers, *Opt. Lett.* **47**, 2979 (2022).
- [12] E. Lucas, G. Lihachev, R. Bouchand, N. G. Pavlov, A. S. Raja, M. Karpov, M. L. Gorodetsky, and T. J. Kippenberg, Spatial multiplexing of soliton microcombs, *Nat. Photonics* **12**, 699 (2018).
- [13] E. Averlant, M. Tlidi, K. Panajotov, and L. Weicker, Coexistence of cavity solitons with different polarization states and different power peaks in all-fiber resonators, *Opt. Lett.* **42**, 2750 (2017).
- [14] R. Suzuki, S. Fujii, A. Hori, and T. Tanabe, Theoretical study on dual-comb generation and soliton trapping in a single microresonator with orthogonally polarized dual pumping, *IEEE Photonics J.* **11**, 6100511 (2019).
- [15] A. U. Nielsen, B. Garbin, S. Coen, S. G. Murdoch, and M. Erkintalo, Coexistence and Interactions between Nonlinear States with Different Polarizations in a Monochromatically Driven Passive Kerr Resonator, *Phys. Rev. Lett.* **123**, 013902 (2019).
- [16] G. Xu, A. U. Nielsen, B. Garbin, L. Hill, G.-L. Oppo, J. Fatome, S. G. Murdoch, S. Coen, and M. Erkintalo, Spontaneous symmetry breaking of dissipative optical solitons in a two-component Kerr resonator, *Nat. Commun.* **12**, 4023 (2021).
- [17] C. Bao, P. Liao, A. Kordts, L. Zhang, A. Matsko, M. Karpov, M. H. P. Pfeiffer, G. Xie, Y. Cao, A. Almain, M. Tur, T. J. Kippenberg, and A. E. Willner, Orthogonally polarized frequency comb generation from a Kerr comb via cross-phase modulation, *Opt. Lett.* **44**, 1472 (2019).
- [18] B. Kostet, Y. Soupart, K. Panajotov, and M. Tlidi, Coexistence of dark vector soliton Kerr combs in normal dispersion resonators, *Phys. Rev. A* **104**, 053530 (2021).
- [19] V. E. Lobanov, A. E. Shitikov, R. R. Galiev, K. N. Min'kov, O. V. Borovkova, and N. M. Kondratiev, Generation of vector flat-top solitons and hybrid bright-flat-top soliton complexes in optical microresonators via modulated pump, *Phys. Rev. A* **104**, 063511 (2021).
- [20] D. J. Kaup, B. A. Malomed, and R. S. Tasgal, Internal dynamics of a vector soliton in a nonlinear optical fiber, *Phys. Rev. E* **48**, 3049 (1993).
- [21] N. Akhmediev, A. Buryak, and J. M. Soto-Crespo, Elliptically polarized solitons in birefringent optical fibers, *Opt. Commun.* **112**, 278 (1994).
- [22] S. T. Cundiff, B. C. Collings, N. N. Akhmediev, J. M. Soto-Crespo, K. Bergman, and W. H. Knox, Observation of Polarization-Locked Vector Solitons in an Optical Fiber, *Phys. Rev. Lett.* **82**, 3988 (1999).
- [23] H. Zhang, D. Y. Tang, L. M. Zhao, X. Wu, and H. Y. Tam, Dissipative vector solitons in a dispersion managed cavity fiber laser with net positive cavity dispersion, *Opt. Express* **17**, 455 (2009).
- [24] S. Fujii and T. Tanabe, Dispersion engineering and measurement of whispering gallery mode microresonator for Kerr frequency comb generation, *Nanophotonics* **9**, 1087 (2020).
- [25] P. Del'Haye, S. A. Diddams, and S. B. Papp, Laser-machined ultra-high-Q microrod resonators for nonlinear optics, *Appl. Phys. Lett.* **102**, 221119 (2013).
- [26] I. S. Grudinina and N. Yu, Dispersion engineering of crystalline resonators via microstructuring, *Optica* **2**, 221 (2015).
- [27] Y. Nakagawa, Y. Mizumoto, T. Kato, T. Kobatake, H. Itobe, Y. Kakinuma, and T. Tanabe, Dispersion tailoring of a crystalline whispering gallery mode microcavity for a wide-spanning optical Kerr frequency comb, *J. Opt. Soc. Am. B* **33**, 1913 (2016).
- [28] A. E. Shitikov, I. A. Bilenko, N. M. Kondratiev, V. E. Lobanov, A. Markosyan, and M. L. Gorodetsky, Billion Q-factor in silicon WGM resonators, *Optica* **5**, 1525 (2018).
- [29] G. Xu, L. Hill, J. Fatome, G.-L. Oppo, M. Erkintalo, S. G. Murdoch, and S. Coen, Breathing dynamics of symmetry-broken temporal cavity solitons in Kerr ring resonators, *Opt. Lett.* **47**, 1486 (2022).
- [30] A. B. Matsko, A. A. Savchenkov, and L. Maleki, On Excitation of breather solitons in an optical microresonator, *Opt. Lett.* **37**, 4856 (2012).
- [31] M. Yu, J. K. Jang, Y. Okawachi, A. G. Griffith, K. Luke, S. A. Miller, X. Ji, M. Lipson, and A. L. Gaeta, Breather soliton dynamics in microresonators, *Nat. Commun.* **8**, 14569 (2017).
- [32] L. A. Lugiato and R. Lefever, Spatial Dissipative Structures in Passive Optical Systems, *Phys. Rev. Lett.* **58**, 2209 (1987).
- [33] A. B. Matsko, A. A. Savchenkov, W. Liang, V. S. Ilchenko, D. Seidel, and L. Maleki, Mode-locked Kerr frequency combs, *Opt. Lett.* **36**, 2845 (2011).
- [34] Y. K. Chembo and C. R. Menyuk, Spatiotemporal Lugiato-Lefever formalism for Kerr-comb generation in whispering-gallery mode resonators, *Phys. Rev. A* **87**, 053852 (2013).
- [35] S. Coen, H. G. Randle, T. Sylvestre, and M. Erkintalo, Modeling of octave-spanning Kerr frequency combs using a generalized mean-field Lugiato-Lefever model, *Opt. Lett.* **38**, 37 (2013).
- [36] A. Pasquazi, M. Peccianti, L. Razzari, D. J. Moss, S. Coen, M. Erkintalo, Y. K. Chembo, T. Hansson, S. Wabnitz, P. Del'Haye, X. Xue, A. M. Weiner, and R. Morandotti, Micro-combs: A novel generation of optical sources, *Phys. Rep.* **729**, 1 (2018).
- [37] G. P. Agrawal, *Nonlinear Fiber Optics*, 6th ed. (Elsevier, Amsterdam, 2019).
- [38] C. Schelte, D. Hessel, J. Javaloyes, and S. V. Gurevich, Dispersive Instabilities in Passively Mode-Locked Integrated External-Cavity Surface-Emitting Lasers, *Phys. Rev. Appl.* **13**, 054050 (2020).